International Journal of Mathematical, Engineering and Management Sciences
Vol. 6, No. 5, 1230-1241, 2021
https://doi.org/10.33889/IJMEMS.2021.6.5.074

Numerical Simulations of Heat Transfer Phenomena through a Baffled Rectangular Channel

Sandip Saha
Department of Mathematics,
National Institute of Technology Silchar, Silchar-788010, Assam, India.
Corresponding author: sandip_rs@math.nits.ac.in, sandip.tfgss@gmail.com

Pankaj Biswas
Department of Mathematics,
National Institute of Technology Silchar, Silchar-788010, Assam, India.
E-mail: pankaj@math.nits.ac.in

Apurba Narayan Das
Department of Mathematics,
Alipurduar University, Alipurduar-736121, West Bengal, India.
E-mail: apuraiganj1964@gmail.com

(Received on February 2, 2021; Accepted on July 12, 2021)

Abstract
In presence of baffle, the turbulent airflow phenomena as well as forced convective heat exchange characteristics in two-dimensional rectangular channel have been analyzed in this work. For variations in Reynolds number (*Re*), we have studied the variations in characteristics of thermal behavior due to the change in the shape of baffle. Computations have been done using finite volume method (FVM) and FLUENT software and the SIMPLE algorithm has been employed for solving the governing equations. Finally, the flow and thermal exchange characteristics viz., streamline flow, turbulence intensity (TE), axial velocity, turbulence kinetic energy (TKE), normalized friction factor (F), normalized average Nusselt number (Nu_{avg}) and thermal enhancement factor (TEF) have been studied in details from numerical standpoint. It has been found that the triangular shaped baffle provides highest value of F at *Re* = 30,000 and at *Re* = 46, 000, the maximum value of the TEF is found for the same baffle implying that triangular shaped baffle is more suitable for overall purposes.

Keywords- Turbulent airflow, Fluent, FVM, SIMPLE algorithm, Thermal exchange characteristic.

1. Introduction

Air is used abundantly for the purpose of internal cooling in several machines like small electronic equipment, solar energy collectors, waste disposal machinery, etc. Apart from these above mentioned equipment's, FVM is extensively used for various commercial purposes such as designing in rooms and workshops, chemical reactors, bio-engineering etc. (Mokhtari et al., 2017; Gaikwad and Parmar, 2020; Nakhchi et al., 2020; Nidhul et al., 2020; Işık and Tuğan, 2021; Saha et al., 2021a; Saha and Das, 2021b). Several techniques are adopted to increase heat transfer substantially for internal cooling in air media so far and among those the most popular and effective technique is to place different shaped baffles in a direction perpendicular to the flow. For that a very complicated air flow, generated in the system, causes disturbance in boundary layer growth and as a result rate of heat exchange increases between the air and boundaries. Using FVM, Kumar and Kim (2015) considered thermal phenomena of turbulent flow in a rectangular micro-channel having periodic ribs. They reported that attachment of ribs in an electronic cooling tube affects significantly F and the Nu_{avg}, which increases the rate of thermal exchange. Employing FVM,

Pirouz et al. (2011) observed conjugate thermal exchange in a rectangular duct embedded with the ribs at upper and lower boundaries and observed that increase in the inter-ribs spacing causes increase in the rate of heat transfer. By FVM, Sripattanapipat and Promvonge (2009) observed the behaviors of periodic flow and heat exchange in a two-dimensional laminar channel having diamond-shaped ribs. They reported that diamond shaped baffle having half apex angle 5^0 to 10^0 provides better results than the flat baffle. Promvonge et al. (2010) numerically solved the problem of the laminar thermal exchange in a square cavity embedded with 45^0 angled baffle on its wall and observed that a single stream wise vortex flow appears and causes impinging jets in the channel wall included between the baffles. Tang and Zhu (2012) observed the fluid flow and the behaviors of heat transfer in a rectangular cavity comprising discrete crossed ribs and grooves and it is shown in their work that the thermo-hydraulic potential in that crossed ribs and grooves channel is enhanced by 9.99% to 13.5% of that of the case of ribbed channel. Employing FVM, Eiamsa-ard et al. (2013) and Smith et al. (2012) studied the impacts of wire coil, twisted tape and circular ring on thermal exchange and pressure drop in flow. For combined tabulator, twisted tape and circular ring, they stated the value of TF is 1.42. Saha (2021) numerically studied different heat transfer characteristics in a rectangular micro-channel having plane and trapezoidal baffles and concluded that plane baffles become less pronounced than trapezoidal baffles. From this literature survey, it is evident that the above mentioned works are based on numerical and experimental observations of turbulent fluid flow and thermal exchange behaviors in presence of plane, flat and periodic baffles in various forms of channel. This work is an extension of the experimental work done by Demartini et al. (2004), where a rectangular channel with a pair of baffles mounted in its walls has been considered and it has been shown that pressure drop increases as *Re* and baffle height increase. Saha et al. (2020) solved the problem based on the flow phenomena in presence of two, three, four rectangular and trapezoidal baffles. At x = 0.448 m and Re=87, 300, they concluded that the axial velocity becomes 2.949 times of inflow velocity for the presence of rectangular baffles whereas in presence of trapezoidal baffle, it becomes 6 times of inflow velocity. In both the works, mentioned above, they did not present any kind of variation in baffle configuration and the most important thing to be noted that both the works considered the fluid flow phenomena only. They have not incorporated the hydro-thermal phenomena and did not consider other forms of baffle in the channel. The above reasons inspired us a lot to study the turbulent characteristics of thermal behavior in presence of baffle of different shapes (plane, trapezoidal, left and right trapezium, triangular and diamond) which has great importance in various engineering communities and industries based on selection of the type of baffle configurations associated with hydro-thermal phenomena.

2. Model Geometry

Recently, in the field of fluid mechanics, strong interests have grown to investigate the flow phenomena in an enclosure. Figure 1 show the cross section of a horizontal rectangular channel with the walls as heated and the bottom wall is embedded with a baffle, such as (a) plane [case-1], (b) trapezoidal [case-2], (c) right sided trapezium [case-3], (d) left sided trapezium [case-4], (e) triangular [case-5] and (f) diamond shape [case-6] in vertical position. Air is injected through the inlet and outlet is on the right side as shown in the Figures 1(a-f). The radiation of heat transfer, body forces, viscous dissipation and Buoyancy effects are neglected. Geometrical dimensions and fluid properties have been chosen like Demartini et al. (2004). To model the geometry and for simulation purpose, the commercial software FLUENT (Gupta et al., 1995; Saha et al., 2020; Saha, 2021) has been employed.

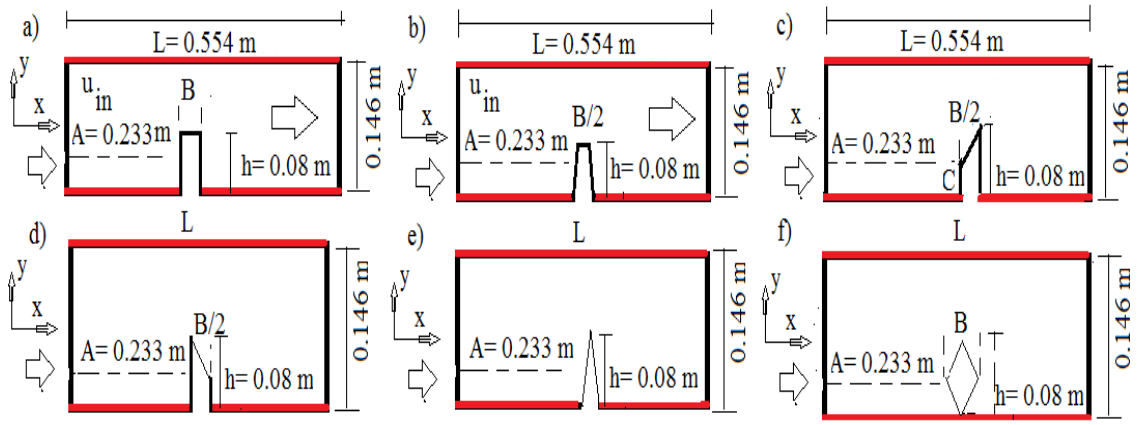

Figure 1. Schematic diagrams of rectangular channel with different forms of baffles.

3. Governing Equation

The steady, incompressible turbulent air flow through the above form of channels is followed by continuity (eq. 1), momentum (eq. 2) and energy (eq. 3) equations (Endres and Möller, 2001).

$$\frac{\partial(\rho.u_i)}{\partial x_i} = 0 \tag{1}$$

$$\frac{\partial(\rho.u_i.u_j)}{\partial x_i} = -\frac{\partial p}{\partial x_i} + \frac{\partial}{\partial x_j}\left[\mu\left(\frac{\partial u_i}{\partial x_j} + \frac{\partial u_j}{\partial x_i} - \frac{2}{3}\,\delta_{ij} * \frac{\partial u_i}{\partial x_j}\right)\right] \frac{\partial}{\partial x_j}\left(-\rho.\overline{u_i u_j}\right) \tag{2}$$

$$\frac{\partial(\rho.u_i.T)}{\partial x_j} = \frac{\partial}{\partial x_j}\left[\left(\frac{\mu}{Pr} - \frac{\mu_t}{Pr_t}\right)\frac{\partial T}{\partial x_j}\right] \tag{3}$$

Where, u_i, u_j, p, $\rho.\overline{u_i u_j}$ and $u_i T$ denote mean velocity components along x_i and x_j directions, pressure, Reynolds stresses and thermal stresses respectively. The Navier-Stokes equations can be solved using (a) Spalart-Allamaras model, (b) k-ϵ model, (c) SST $k-\omega$ model and (d) Reynolds stress model. To investigate flow phenomena in the vicinity and far-off the walls, SST $k-\omega$ model (Spalding, 1974) is useful to achieve the accurate results (Gupta et al., 1995; Ko and Anand, 2003; Skullong et al., 2017) for the presence of cross diffusion term, blending function and SST $k-\omega$ model (Saha, 2021) is useful for changing interior of boundary layer and is transformed to k- ω model at higher values of *Re* (Endres and Möller, 2001; Nasiruddin and Siddiqui, 2007). The SST k-ω model contains following equations involving turbulence kinetic energy (k_{tr}) and dissipation rate (ω).

$$\frac{\partial(\rho.k_{tr}.u_i)}{\partial x_i} = \frac{\partial}{\partial x_j}\left[\Gamma_k\left(\frac{\partial k_{tr}}{\partial x_j}\right)\right] - \rho\overline{u_i' u_j'}\frac{\delta u_j}{\delta x_i} + S_k - \rho * 0.072 * \left(1 + 0.05 * F(M_t)\right) f_\beta{}^* k\omega \tag{4}$$

Here ρ, G_k, G_ω, Γ_k, Γ_ω, S_k, S_ω and D_ω denote density (kg.m^{-3}), turbulence kinetic energy generation due to the gradient of mean velocity, generations of ω, effective diffusivity of k and ω, turbulence and the dissipation term of k, ω, the user defined source terms, cross diffusion terms and these terms have been prescribed according to FLUENT user guide (Patankar, 1980; Gupta et al., 1995; Ko and Anand, 2003; Saha, 2021; Mahendran, 2021). The expressions for Γ_k, Γ_ω, α^*, $f_\beta{}^*$ and $F(M_t)$

are given in Endres and Möller (2001). The parameters have been described, $Re = \frac{\rho d_h u}{\mu}$, absolute pressure drop, $\mathbf{\Delta}p = |p_{out} - p_{in}|$, friction factor, $f = \frac{2d_h \Delta p}{\rho {u_{in}}^2}$, $Nu = \frac{1}{0.554}\int_0^L Nu_x\, dx$, $Nu_{avg} = \frac{Nu}{Nu_0}$, $F = \frac{f}{f_0}$, $TEF = \frac{Nu}{Nu_0}\left(\frac{1}{F}\right)^{\frac{1}{3}}$ with d_h = hydraulic diameter as mentioned in Demartini et al. (2004), u_{in} = average velocity and f_0 is the friction factor.

$$\frac{\partial(\rho.\omega.u_i)}{\partial x_i} = \frac{\partial}{\partial x_j}\left[\lceil_\omega\left(\frac{\partial \omega_{tr}}{\partial x_j}\right)\right] + \frac{\alpha_\infty}{\alpha^*}\left(\frac{\left(0.024+\rho.k.(2.95\mu.\omega)^{-1}\right)}{(1+\rho.k.(2.95\mu.\omega)^{-1})}\right) + S_\omega - \rho * 0.072 * \left(1 - 1.3125 * \left(\frac{\left(0.26+(\rho.k)^4.(8\mu.\omega)^{-4}\right)}{((1+(\rho.k)^4.(8\mu.\omega)^{-4}))}\right) * F(M_t) * \left(\frac{1+70*\left(\left|\left(\Omega_{ij}\Omega_{jk}S_{ki}\right).(\beta^*{}_\infty.\omega)^{-3}\right|\right)}{1+80*\left(\left|\left(\Omega_{ij}\Omega_{jk}S_{ki}\right).(\beta^*{}_\infty.\omega)^{-3}\right|\right)}\right)\right)\omega^2 + D_\omega \quad (5)$$

For $Re \geq 10^4$, Nusselt number taken as per the work of Dittus and Boelter (1985):

$$Nu_0 = 0.023 * Re^{0.8} * Pr^{0.4} \quad (6)$$

From the Petukhov (1970) correlation form, the following result has been taken:

$$f_0 = (0.79 * lnRe - 1.64)^{-2}, \text{when } 3 \times 10^3 \leq Re \leq 5 \times 10^6 \quad (7)$$

3.1 Boundary Conditions and Computational Procedures

Like Demartini et al. (2004), the hydrodynamic boundary conditions have been specified and the thermal boundary conditions have been chosen like Nasiruddin and Siddiqui (2007). Uniform velocity distribution (y = 0; u_{in}) has been prescribed at the inlet section and the fluid temperature has been kept at 27^0C. No slip and no penetration boundary conditions (u = 0; v = 0) have been applied at the channel walls (y = 0.073m, y = -0.073m) and pressure outlet with zero gauge pressure has been taken as outlet boundary conditions. The walls of the computational domain have been assumed to be heated 102^0C. The major advantage of FVM is its simplicity for formulation of an unstructured mesh and for this FVM (Marzouk et al., 2020; Mohammadi et al., 2020; Nakhchi et al., 2020; Nidhul et al., 2020; Saha et al., 2020) is employed for solving the governing equations describing the hydro-thermal phenomena. SIMPLE algorithm has been used to develop the primitive variables (pressure and velocity) of the governing equations and for convective terms, the second order upwind scheme has been employed. To achieve the high velocity gradient, pressure and temperature, the grid has been selected as non-uniform and highly dense near the baffles. In addition, for all the dependent variables, the convergence criteria have been set as 10^{-9}. FVM evaluates a PDE reducing it to a system of algebraic equations. Triple integrals containing divergence term are transformed into double integrals using divergence theorem. In this method a mesh is constructed like finite element method, which consists of a partition of domain. The mesh elements are termed as volumes. Integration of the PDE over each mesh yields a balance equation and the system of such equations is then discretized with respect to a set of discrete unknowns. The main issue is discretization of fluxes at the boundaries of each control volume. The working procedures are described as below:

(i) Divide the domain into a number of sub domains of finite size and each of those is represented by finite number of grid points.
(ii) Integrate the governing differential equation over each sub domain.

(iii) Consider a profile assumption for the dependent variable for evaluating the integrals for expressing the results in terms of algebraic quantities at the grid points.

3.2 Test of Grid and Validation of Code

To find the influence of grid sizes on the findings, a grid independence test has been conducted at *Re* = 87, 300 on a rectangular micro-channel as considered by Demaritini et al. (2004). Figure 2(a), depicts that as the number of elements exceeds 20,000, average pressure coefficients become constant implying that 20,000 numbers of elements are sufficient for future analysis. The validation of the code has been done using the experimental geometry considered and the boundary conditions prescribed in the work of Demaritini et al. (2004).

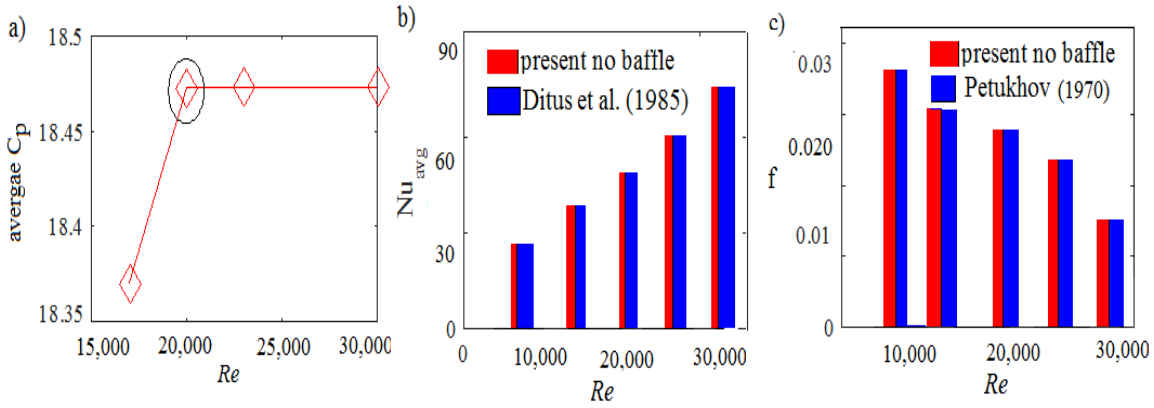

Figure 2. Profiles of average C_p, Nu_{avg} and f with *Re*.

In absence of baffle, Figures 2(b-c), represent a strong agreement between the results of Dittus and Boelter (1985), Petukhov (1970) and present work. In addition, at *Re*=87,300, validation of this work has been done with Demartini et al. (2004) [Figures 3(a-b)], numerical work of Saha et al. (2020) [Figure 3(c)] and Saha (2021) [Figure 3(d)] in presence of the rectangular baffles. Profiles of normalized velocity have been presented at different locations given by x = 0.159 m [Figure 3(a)], 0.189 m [Figure 3(b)], 0.289 m [Figure 3(c)] and 0.525 m [Figure 3(d)] and Table 1 presents the percentage error at various locations (x = 0.255 m; 0.285 m). Figures 2(b-c), 3(a-d) and Table 1 show that the results of this work are too closed to those of the experimental works of Petukhov (1970), Dittus and Boelter (1985), Demartini et al. (2004), numerical works of Saha et al. (2020), Saha (2021) which provide enough confidence to continue the present study.

Table 1. % Error of Demartini et al. (2004) vs current study.

Normalized velocity at x= 0.255 m			
Demartini et al. (2004)	**current study**	**% error**	**Total % error**
-0.0065811	-0.00657	0.160	0.608
0.00294847	0.00294	0.287	
0.0805	0.080337	0.161	

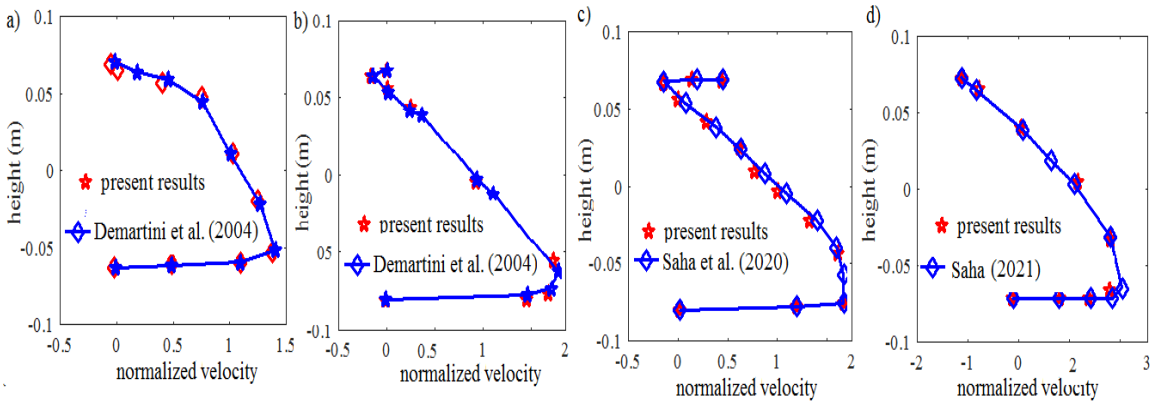

Figure 3. Profiles of normalized velocity vs. different locations at *Re* = 87,300.

4. Results and Discussion

4.1 Streamlines and Turbulent Kinetic Energy (TKE)

In Figure 4, streamlines are drawn for the channels with different shaped baffles for *Re*= 20,000 [Figures 4.(a-f)] and 1, 00, 000 [Figures 4.(g-l)] respectively. From those Figures, we see that two main regions exist. First one is found as the passage over the baffle where the flow gets accelerated as the flow area reduces and the stream lines get deflected. The second one is identified as the base of the baffle where the stream lines are found due to flow expansion and a recirculation flow, directly proportional to *Re*, is formed there. The air is pushed regularly through the inlet and small weak zones are formed in the base of the baffle due to the loss in pressure there. It is also observed that two reverse weak zones are formed behind the baffle at *Re* =20,000, as can be seen in case-5 of Figure 4. It is to be noted further that for a higher *Re* (*Re*= 1, 00, 000) length of weak zone is elongated due to the presence of the same baffle (in case-5 of Figures 4(g-l)]) where an irregular flow is observed behind the baffle. It is observed that the flow is uniform until it reaches the first baffle of any form, where the recirculation of flows is developed. Baffle prevents the fluid flow and diminishes the primary vortex. Diagrams 4(a-l) present the existence of clockwise vortex at the upstream section of the baffle. After passing through the passage over the baffle, the flow directly strikes on that wall and forms a recirculation zone inside the inter baffle groove. The rest of fluid get accelerated and causes the existence of second vortex at the base behind the baffle**.** At location x=0.395m and for *Re* = 1,00,000, it has been found that maximum velocity attains approximately 3.23, 3.2, 1.04, 3.26, 3.32 and 3.19 times of reference velocity. Figures 5[a-l] respectively exhibit the change in TKE for different shapes of baffle for *Re* = 20,000 and 1, 00,000 and this is found very low in the zone lying in front of the baffle for all the cases. The kinetic energy enhances as the flow moves forward through the passage over the baffle and the same thing happens with the increase in *Re*. Maximum value of TKE is observed in Figure 5(e) and 5(k) while the lowest value of that found in Figure 5(c), 5(i). At *Re*=1,00,000, the highest values of TKE found in case 3 are 18, 16, 17.94, 34 and 17.96 times lower than that of the case-1, case-2, case-4, case-5 and case-6 respectively.

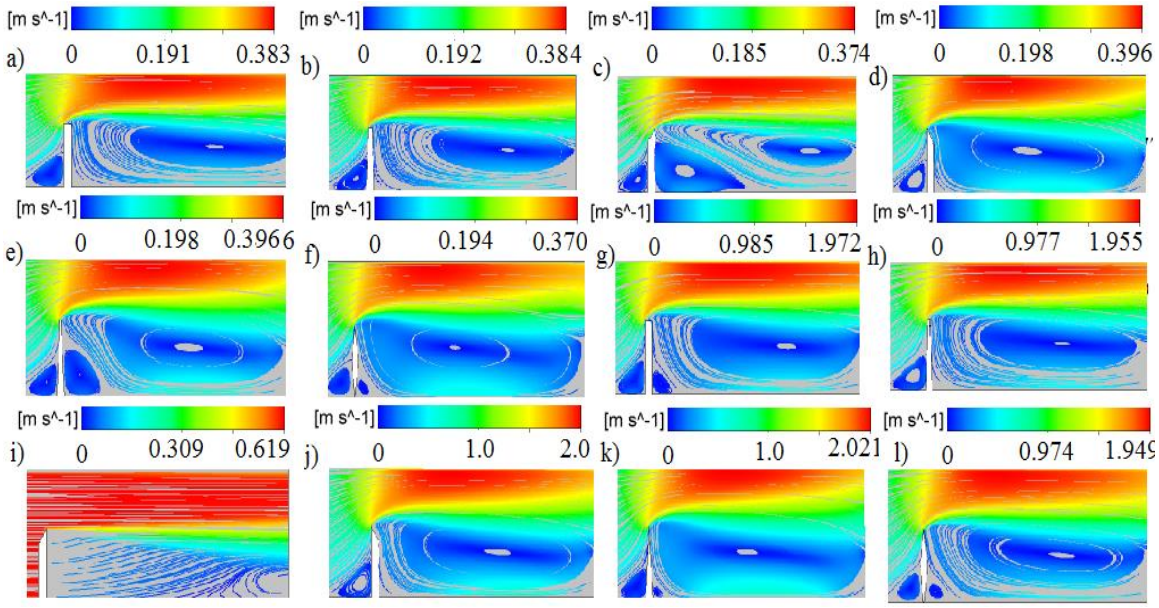

Figure 4. Streamlines for different baffles at *Re* = 20, 000 [a-f] and *Re*= 1, 00, 000 [g-l].

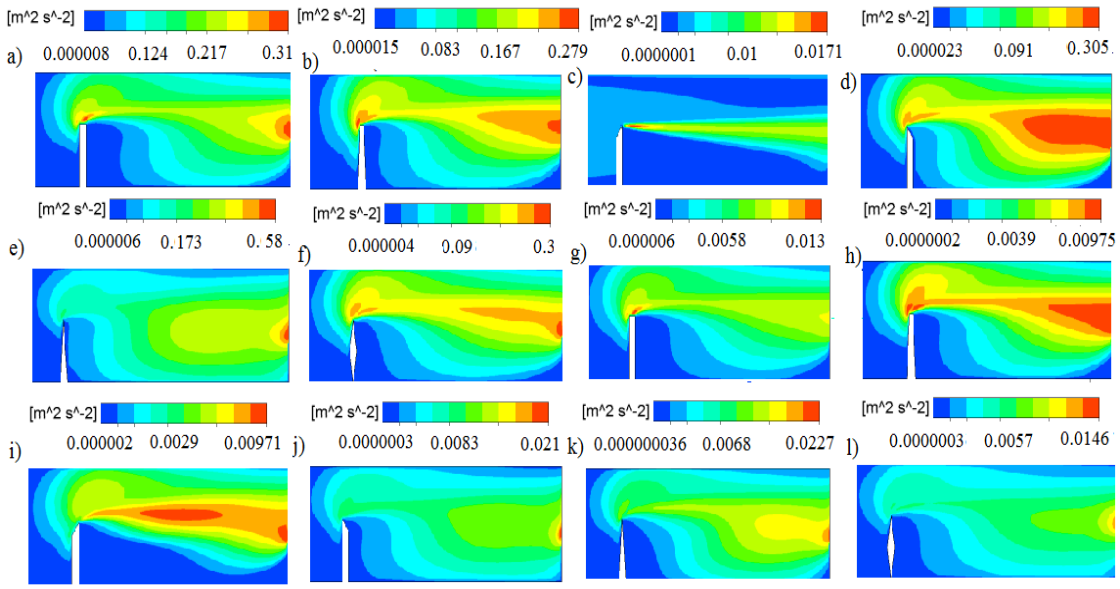

Figure 5. Profiles of TKE for different baffles at *Re* = 20, 000 [a-f] and *Re* = 1, 00, 000 [g-l].

4.2 Turbulence Intensity and Axial Velocity

Figure 6 exhibit the contours of turbulence intensity for different values of *Re* (*Re* =20,000, 1, 00, 000) in the enclosures with different shaped baffles. This disturbance in flow, caused by the baffle, changes the flow direction towards the heated walls and for which the intensity in turbulence augmented especially behind the baffle, however, turbulence intensified substantially for increase

in *Re*. In this setup, highest turbulence intensity observed in Figure 6(k) whereas the Figure 6(f) shows the least intensity. At the tip of baffle, the axial velocity rises suddenly and continues along the upper wall till it becomes very low near the lower wall after crossing the obstacle. It is important to note that the right-handed trapezium shaped baffle lets the air to blow with higher speed, even in the outlet. As expected, it is found in both the Figures 7[a-l] that axial velocity becomes very low at the base area behind the baffle. The negative axial velocity assures the existence of reverse recycling cells at the lower regions surrounding the baffles for all the cases as shown in Figures 7[a-l] except in Figure 7(i), where the axial velocity is found to be uniform throughout the enclosure. A moderate axial speed is observed near the outlet and as expected, comparatively higher axial velocity exists for higher *Re*. The highest axial velocity found for *Re* = 20, 000 is equal to 0.397 m/s as shown in Figure 7(e), whereas for *Re* = 1, 00, 000, the magnitude of the speed increases up to 2.02 m/s (Figure 7k). In case-5, maximum axial velocity is found 2.02 m/s, which decreases by 2.5%, 3%, 6.9%, 1% and 3% in case-1, case-2, case-3, case-4 and case-6 respectively at *Re*=1, 00, 000. It is also revealed that the corrugated baffle may elongate the flow path and strengthen vortex more for change in velocity. Flow patterns drawn for different values of *Re* are almost similar (refer Figure 7) except in the region around the tip of the baffles. The flow accelerates as it proceeds towards the outlet of the channel and the size of the weak region increases with the rise in flow velocity. From the Figures 7(a-f) and 7(g-l), it is seen that flow velocity becomes very low in the neighborhood of the baffle, particularly at its base for the formation of recirculation there and faraway of this region, the current lines become collateral and generate continuous flow. It is to be noted also that mean velocity increases at the passage over the baffle. The axial velocity increases due to the existence of both baffle and recirculation and for that flow direction changes suddenly.

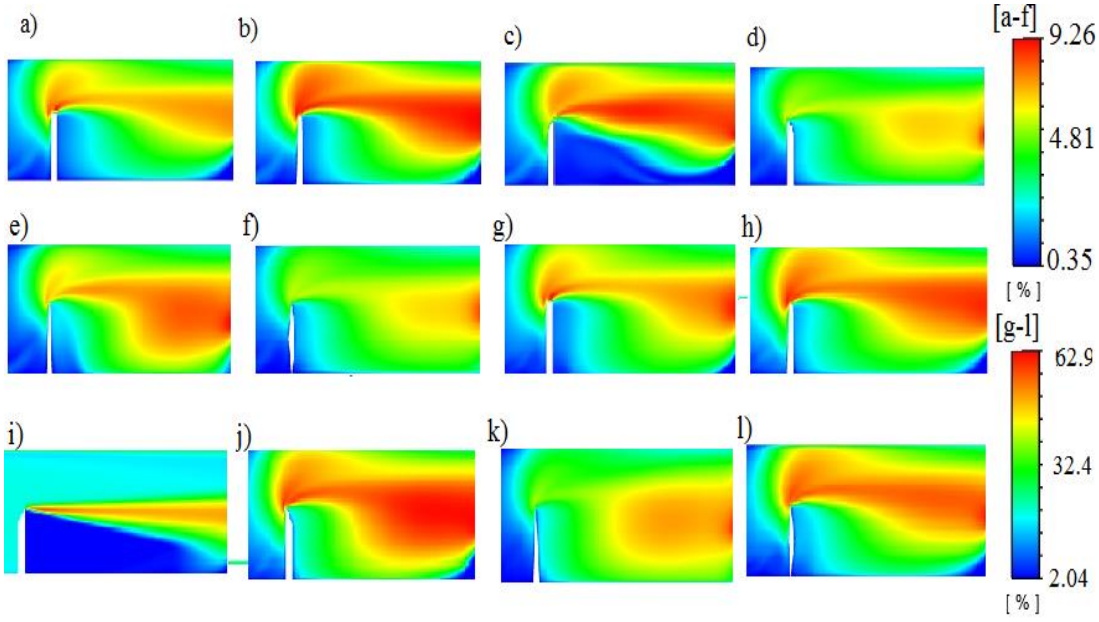

Figure 6. Profiles of TE for at *Re* = 20, 000 [a-f] and at *Re* = 1, 00, 000 [g-l].

4.3 Variation of F, Nu_{avg} and TEF

The presence of baffle affects velocity field, pressure but the latter is associated with the penalty of **Δ**p in terms of F (Figure 8(a)) and also the arrangement of baffles affects heat transfer.

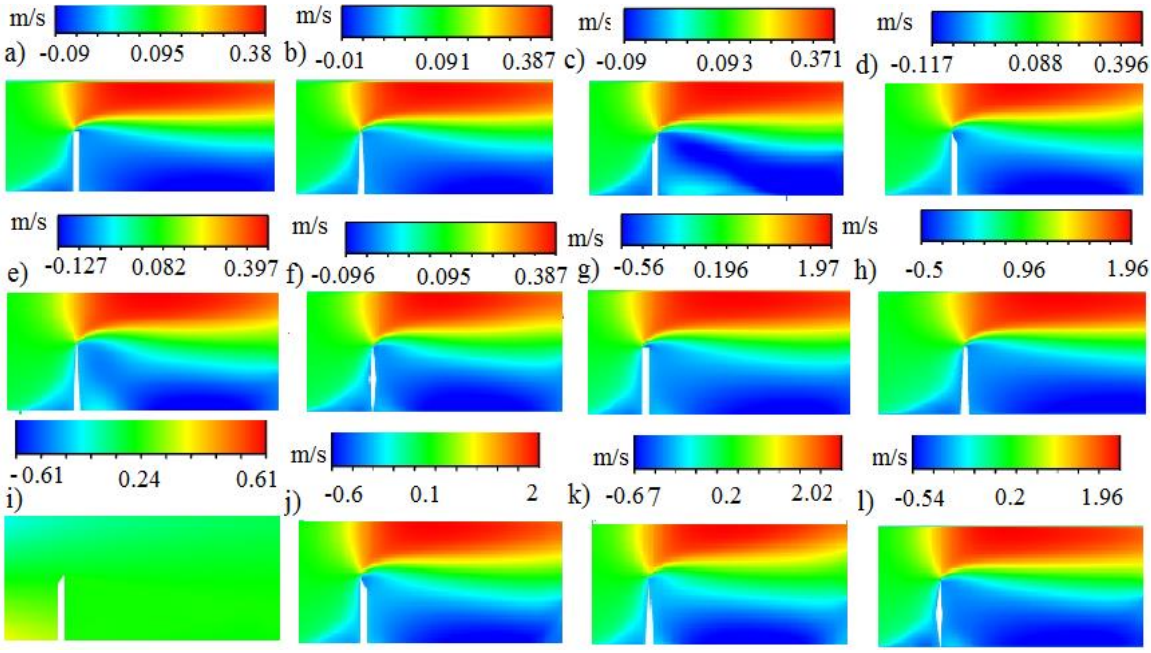

Figure 7. Profiles of axial velocity for different baffles at *Re* = 20, 000 [a-f] and at *Re* = 1, 00, 000 [g-l].

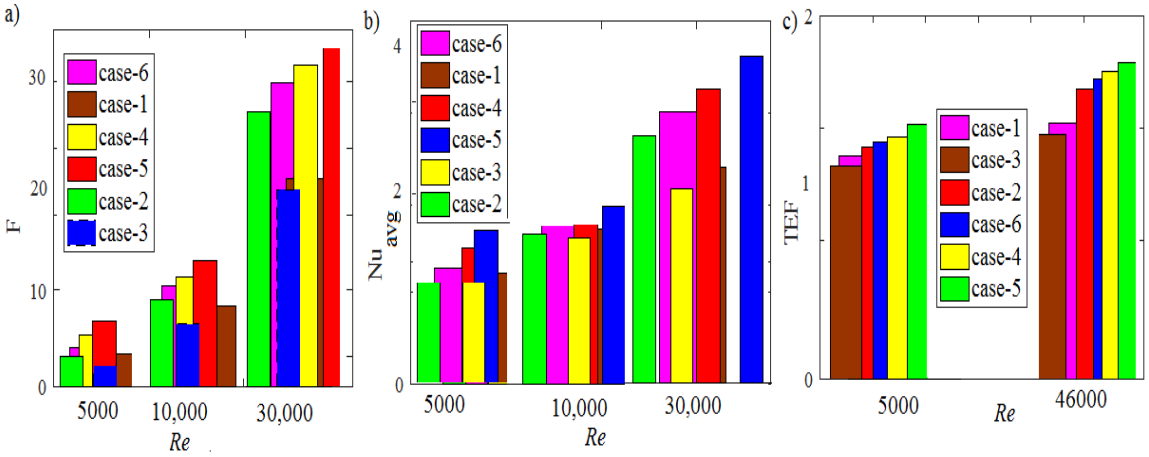

Figure 8. Profiles of F (a), Nu_{avg} (b) and TEF (c) with different *Re* for different baffles.

As expected, the value of F increases as *Re* increases and the maximum drop in pressure occurs at y = 0.073 m, indicating that more resistance to flow subsists there. The convective heat transfer from channel wall to air increases its velocity. Figure 8(b) depicts the effect of *Re* on the evolution of the values of Nu_{avg}. As the velocity gradient is high at the upper boundary of the channel, the greatest variations in Nu_{avg} are found there. Thermal enhancement concerns a friction coefficient

penalty that causes increase in △p. Figure 8(a) exhibits the profile of F against *Re* for all the cases. For large values of *Re*, it is found that increase in the heat transfer rate becomes high with the increase in flow rate and the temperature drops substantially. In case-5, we see that the friction factor becomes approximately 1.04, 1.13, 1.2, 1.44 and 1.54 times of that of case-4, case-6, case-2, case-1, and case-3 respectively at *Re* = 30, 000. The variations of Nu_{avg} with *Re* in an enclosure with various forms of baffle are presented in Figure 8(b) and found that Nu_{avg} increases as *Re* increases. At *Re* = 30,000, it has been noted that the case-5 (triangular shaped baffle) provides highest value of F which is about 13.4%, 16.5%, 21.3%, 36.2%, 41.34% higher than that of the case-4, case-6, case-2, case-1 and case-3 respectively. Implementation of the concept of TEF is important for thermal and kinetic efficiency. Figure 8(c) depicts the change in TEF in an enclosure against the *Re* for different types of baffles. At *Re* = 46, 000, the TEF is found to be maximum, which is nearly 1.825 in case-5 and this reduces by 4%, 9.5%, 13.4%, 17.9% and 22% in the case-4, case-6, case-2, case-1 and case-3 respectively.

5. Conclusions

Numerical studies on turbulent airflow phenomena in a rectangular channel with various forms of baffle (plane, trapezoidal, left and right trapezium, triangular and diamond) and on the characteristics of thermal behavior have been done. The geometry of this work is based on the baffle configurations used in heat exchanger shell and tube. Needless to say that this study has great importance in various engineering communities and industries which are based on selection of the type of baffle configurations associated with hydro-thermal phenomena. The concluding remarks are as below:

a) It is observed that an increase in *Re* induces increase in F, Nu_{avg} and TEF. It has also been found that vortex shedding creates the existence of low and high-pressure regions. In the presence of different shaped baffles, it is realized that the highest friction factor appears in fifth case while the lowest friction factor arises in first and third cases.
b) The rise in Nusselt number for enhancing *Re* is found to be highest in case-5 while case-3 provides the lowest rise in Nusselt number in comparison to the other cases. At *Re* = 30,000, it has been observed, triangular shaped baffle provides highest value of F which is about 13.4%, 16.5%, 21.3%, 36.2%, 41.34% higher than that of the case-4, case-6, case-2, case-1 and case-3 respectively. It is also noted that at *Re* = 46, 000, the TEF is found to be maximum in the case-5 and this reduces by 4%, 9.5%, 13.4%, 17.9% and 22% in the case-4, case-6, case-2, case-1 and case-3 respectively.

Thus the findings of this work indicate that by incorporating the baffles into the flow, an increase in heat transfer in large amount in a heat exchanger tube is possible and this concept can be utilized in different engineering equipments as per need. In addition to that we see that among all the form of baffles, the baffle defined in case-5, i.e., triangular baffle is found more suitable for overall purposes.

Conflict of Interest

The authors declare that there is no conflict for this publication.

Acknowledgments

Authors wish to thank the reviewers for their suggestions on the improvement of this work and Mr. Sandip Saha thankfully acknowledges the financial support from Ministry of Education, formerly the Ministry of Human Resource Development, Government of India to carry out the work.

References

Demartini, L.C., Vielmo, H.A., & Möller, S.V. (2004). Numeric and experimental analysis of the turbulent flow through a channel with baffle plates. *Journal of the Brazilian Society of Mechanical Sciences and Engineering*, *26*(2), 153-159.

Dittus, F.W., & Boelter, L.M.K. (1985). Heat transfer in automobile radiators of the tubular type. *International Communications in Heat and Mass Transfer*, *12*(1), 13-22.

Eiamsa-ard, S., Kongkaitpaiboon, V., & Nanan, K. (2013). Thermo-hydraulics of turbulent flow through heat exchanger tubes fitted with circular-rings and twisted tapes. *Chinese Journal of Chemical Engineering*, *21*(6), 585-593.

Endres, L., & Möller, S. (2001). On the fluctuating wall pressure field in tube banks. *Nuclear Engineering and Design*, *203*(1), 13-26.

Gaikwad, S., & Parmar, A. (2020). Numerical simulation of the effect of baffle cut and baffle spacing on shell side heat exchanger performance using CFD. *Chemical Product and Process Modeling*, *16*(2), 145-154.

Gupta, B.B., Howell, J.A., Wu, D., & Field, R.W (1995). A helical baffle for cross-flow microfiltration. *Journal of Membrane Science*, *102*, 31-42.

Işık, E., & Tuğan, V. (2021). Investigation of the effect of baffle cut on heat transfer and pressure drop in shell and tube heat exchanger using CFD. *Heat Transfer Research*, *52*(10), 1-18.

Ko, K.H., & Anand, N.K. (2003). Use of porous baffles to enhance heat transfer in a rectangular channel. *International Journal of Heat and Mass Transfer*, *46* (22), 4191-4199.

Kumar, A., & Kim, M.H. (2015). Convective heat transfer enhancement in solar air channels. *Applied Thermal Engineering*, *89*, 239-261.

Mahendran, J. (2021). Experimental analysis of shell and tube heat exchanger using flower baffle plate Configuration. *Materials Today: Proceedings*, *21*(1), 419-424.

Marzouk, S.A., Abou Al-Sood, M.M., El-Said, E.M.S., & El-Fakharany, M.K. (2020). Effect of wired nails circular-rod inserts on tube side performance of shell and tube heat exchanger: Experimental study. *Applied Thermal Engineering*, *167*, 114696.

Mohammadi, M.H., Abbasi, H.R., Yavarinasab, A., & Pourrahmani, H. (2020). Thermal optimization of shell and tube heat exchanger using porous baffles. *Applied Thermal Engineering*, *170*, 115005.

Mokhtari, M., Gaardobary, M.B., Yaganesh, R., & Fallah, K. (2017). Numerical study of mixed convection heat transfer of various fin arrangements in a horizontal channel. *Engineering Science and Technology, an International Journal*, *20*(3), 1106-1114.

Nakhchi, M.E., Esfhani, J.A, & Kim, K.C. (2020). Numerical study of turbulent flow inside heat exchangers using perforated louvered strip inserts. *International Journal of Heat and Mass Transfer*, *148*, 119143.

Nasiruddin, & Siddiqui, M.H.K. (2007). Heat transfer augmentation in a heat exchanger tube using a baffle. *International Journal of Heat and Fluid Flow*, *28*(2), 318-328.

Nidhul, K., Kumar, S., Yadav, A.K., & Anish, S. (2020). Enhanced thermo-hydraulic performance in a V-ribbed triangular duct solar air heater: CFD and exergy analysis. *Energy*, *200*, 117448.

Patankar, S.V. (1980). *Numerical heat transfer and fluid flow*. Hemisphere, New York, London.

Petukhov, B.S. (1970). Heat transfer and friction in turbulent pipe flow with variable physical properties. In: Hartnett, J.P., Irvine Jr., T.F. (eds) *Advances in Heat Transfer*. Elsevier, New York, Vol. 6, pp. 503-564.

Pirouz, M.M., Farhadi, M., Sedighi, K., Nemati. H., & Fattahi, E. (2011). Lattice boltzmann simulation of conjugate heat transfer in a rectangular channel with wall-mounted obstacles. *Scientia Iranica, 18*(2), 213-221.

Promvonge, P., Sripattanapipat, S., Tamna, S., Kwankaomeng, S., & Thianpong, C. (2010). Numerical investigation of laminar heat transfer in a square channel with 45^0 inclined baffles. *International Communications in Heat and Mass Transfer, 37*(2), 170-177.

Saha, S. (2021). Numerical simulation of turbulent airflow and heat transfer through a rectangular channel along with trapezoidal baffle plates. In *AIP Conference Proceedings* (Vol. 2341, pp. 1-10). AIP. Perpignan, France.

Saha, S., & Das, A.N. (2021b). Flow bifurcation phenomena of shear-thinning and newtonian fluids in a rectangular channel in presence of intermediate steps: using Carreau-Yasuda model. *Journal of Applied fluid Mechanics, 14*(4), 1283-1293.

Saha, S., Biswas, P., Nath, S., & Singh, L. (2020). Numerical simulations of Newtonian fluid flow through a suddenly contracted rectangular channel with two different types of baffle plates. *Soft Computing, 25*, 9873-9885.

Saha, S., Biswas, P., Raut, S., & Das, A.N. (2021a). Convective heat transfer of laminar nano-fluids flow through a rectangular micro-channel with different types of baffle-corrugation. *International Journal for Computational Methods in Engineering Science and Mechanics, 22*(2), 1-13.

Skullong, S., Promvonge, P., Thianpong, C., Jayranaiwa, N., & Pimsarnbet, M. (2017). Heat transfer augmentation in a solar air heater channel with combined winglets and wavy grooves on absorber plate. *Applied Thermal Engineering, 122*, 268-284.

Smith, E.A., Koolnapadol, N., & Promvonge, P. (2012). Heat transfer behavior in a square duct with tandem wire coil element insert. *Chinese Journal of Chemical Engineering, 20*(5), 863-869.

Spalding, D.B. (1974). The numerical computation of turbulent flow. *Computer Methods in Applied Mechanics and Engineering, 3*, 269-279.

Sripattanapipat, S., & Promvonge, P. (2009). Numerical analysis of laminar heat transfer in a channel with diamond-shaped baffles. *International Communications in Heat Mass Transfer, 36*(1), 32-38.

Tang, X., & Zhu, D. (2012). Experimental and numerical study on heat transfer enhancement of a rectangular channel with discontinuous crossed ribs and grooves. *Chinese Journal of Chemical Engineering, 20*(2), 220-230.